Journal of Physics: Conference Series **525** (2014) 012018 doi:10.1088/1742-6596/525/1/012018

Separation & free-stream turbulence: implications for surface aerodynamics & heat transfer

J P J Stevenson[1], E J Walsh[2], K P Nolan[3] and M R D Davies[1]

[1] Stokes Institute, University of Limerick, Limerick, Ireland
[2] Department of Engineering Science, University of Oxford, Oxford, UK
[3] Bell Labs Ireland, Thermal Management Research Group, Alcatel-Lucent, Dublin, Ireland

E-mail: jonathan.stevenson@ul.ie

Abstract. Preliminary results from a Particle Image Velocimetry (PIV) investigation of the separation-reattachment flow over a flat plate are presented. The experiments address the effects of two key variables: flow approach angle (manipulated indirectly with a trailing edge flap) and free-stream turbulence level (introduced upstream with grids). The plate thickness Reynolds number is fixed throughout and lies within the transitional regime.

In the first test series (I), it is shown that increasing the turbulence level and reducing the approach angle cause the mean leading-edge separation bubble to shrink. The effect of free-stream turbulence, in particular, diminishes progressively as its level is raised. In the second series (II), downstream development of the reattached boundary layer is found to unfold rapidly at first but plateau after approximately three bubble-lengths. Momentum thickness Reynolds and Stanton numbers develop independently of the free-stream turbulence thereafter, and are well described by shifted turbulent correlations. Heat transfer potential ultimately depends upon the balance between frictional loss, bubble size and downstream mixing.

1. Introduction

Many industrial heat-exchanging surfaces operate at Reynolds numbers and angles of attack high enough to produce regions of transitional separation at their upstream side. In these cases, the flow detaches at the leading edge of the surface, undergoes transition and reattaches as a developing turbulent boundary layer [1].

The region enclosed by the separated layer is known as a *separation bubble*. The bubble recirculates under shear and inhibits local heat transfer by its own thermal inertia. Downstream, recovery of the reattached wall layer to turbulent equilibrium is notably slow [2] and depends, amongst other factors, on surface geometry, upstream approach incidence and streamwise pressure gradient [3]. But under suitable conditions, the enhanced diffusion *might* provide a workable means for increasing heat transfer.

In the present work, Particle Image Velocimetry (PIV) is used to study the effects of upstream approach angle and free-stream turbulence on such a flow for a nominal thickness Reynolds number Re_I ($= U_I D/\nu$) of 480. Two studies are conducted: the first, denoted 'series I', provides time-mean and instantaneous views of the bubble zone. The second, denoted 'series II', focuses on the mean development and heat transfer characteristics of the reattached wall layer.

2. Experimental facility

All measurements were performed in a subsonic open-return wind tunnel facility. The tunnel has a honeycomb-mesh screen cascade at its inlet and a four-square bank of axial fans (in suction mode) at its outlet. The background turbulence level in the test section is 0.7 %. The PIV system consists of a 200 mJ pulsed laser and full-frame 11 MP CCD camera (with a 105 mm f/2.8 macro lens) mounted separately on three-axis traverse platforms. Seeding is provided by a commercial fog generator. Figure 1 shows the arrangement.

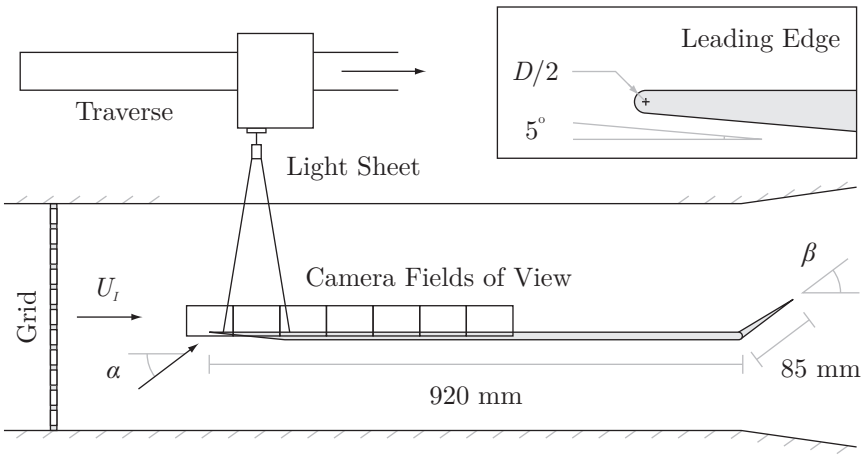

Figure 1: Schematic of the PIV test setup (not to scale).

The round-nosed plate model (295 mm wide × 920 mm long) has a hinged flap at its trailing edge. This allows the circulation, and therefore the upstream approach incidence α of the flow, to be varied indirectly. The flow separates at the leading edge until the flap is positioned at an upward setting β of about 45°, for which an attached *Blasius* boundary layer is produced downstream (figure 2). Note that coordinate x is measured from the leading edge of the plate.

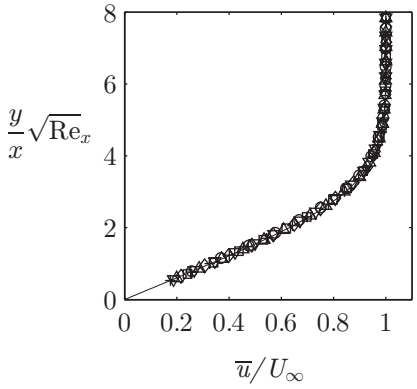

Figure 2: Boundary layer velocity profiles at the 45° flap setting. —— Blasius; ○ $\mathrm{Re}_x = 50100$; □ $\mathrm{Re}_x = 62700$; ♢ $\mathrm{Re}_x = 74900$; △ $\mathrm{Re}_x = 87300$; ▽ $\mathrm{Re}_x = 100000$; + $\mathrm{Re}_x = 111900$.

Free-stream turbulence may be introduced upstream of the plate using grids (with square bars of width d). Figures 3 and 4 show the development of streamwise turbulence intensity T_u, micro-scale λ_x and integral scale Λ_x for the grids of the present study. Roach's correlations [4]

are also shown. Power spectra were further computed at each station and it was confirmed, by comparison with von Kármán's spectrum, that the turbulence was sufficiently isotropic.

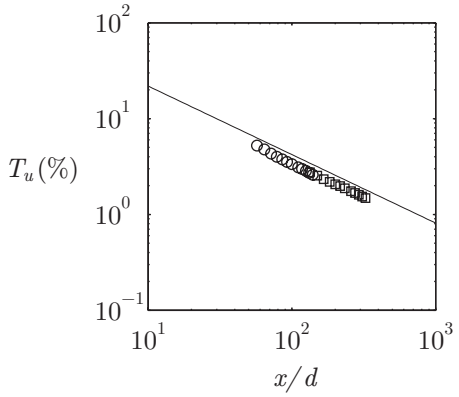

Figure 3: Decay of streamwise intensity T_u. ○ Coarse Grid; □ Fine Grid; —— Roach's [4] square-bar grid correlation.

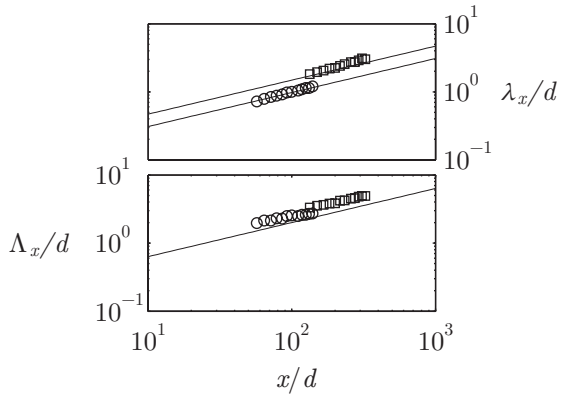

Figure 4: Growth of length scales Λ_x and λ_x. ○ Coarse Grid; □ Fine Grid; —— Roach's [4] length-scale correlations.

Table 1: Series I test cases.

T_u (%)	$[\lambda_x \quad \Lambda_x]$ (mm)	β (α) (°)	Re_I
0.7	—	0 (30)	480
0.7	—	15 (26)	480
0.7	—	30 (20)	480
3.1	[4.8 9.1]	0 (28)	460
3.1	[4.8 9.1]	15 (24)	500
3.1	[4.8 9.1]	30 (19)	480
6	[4.7 13.2]	0 (29)	460
6	[4.7 13.2]	15 (25)	480
6	[4.7 13.2]	30 (20)	490

Table 2: Series II test cases.

T_u (%)	$[\lambda_x \quad \Lambda_x]$ (mm)	β (α) (°)	Re_I
0.7	—	0 (33)	480
0.7	—	22.5 (25)	480
5.7	[4.8 13.5]	0 (33)	460
5.7	[4.8 13.5]	22.5 (24)	480

3. Results

Details of the respective experiment series are provided in tables 1 and 2. Note that the values of T_u, λ_x and Λ_x refer to those at the plate leading-edge station.

3.1. Bubble structure (series I)

Figure 5 shows a vector-contour map of mean absolute velocity $\overline{\mathbf{V}}$ within the leading edge bubble for the 0° flap background-turbulence case. This flow field was representative of all separation bubbles from series I. The coordinate origin was placed at the nose-plate junction and the downstream terminus of the zero-contour for mean streamwise velocity $\overline{u}$, relative to this origin, was used to define the bubble length l_R. Spatial coordinates were normalised accordingly.

The vector detail reveals finely the internal structure of the bubble. The flow entrains under free-stream shear around an apparent centre, for this case, of $x/l_R = 0.75$, and in a time-mean sense is practically enclosed (whilst this perspective masks the complex nature of transitional

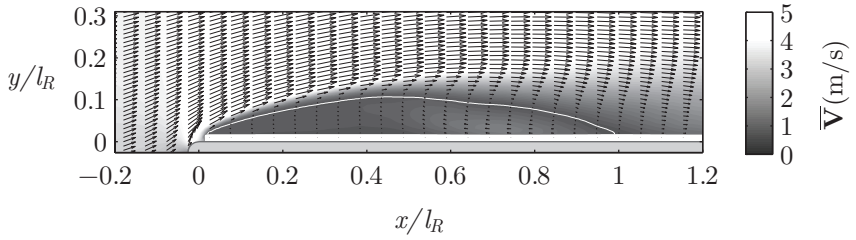

Figure 5: Time-mean PIV absolute velocity vector-contour map of the 0° flap bubble. The $\overline{u}$ zero-contour is shown by the white line and the plate surface is coloured in grey. $l_R = 39$ mm.

shedding, it does serve to illustrate the recirculation mechanism responsible for inhibiting local heat transfer). At reattachment, the mean velocity profile is highly inflectional, but the shearing effect of the wall—which effects the growth of a new 'inner' layer—gradually initiates a return to fuller form (see section 3.2).

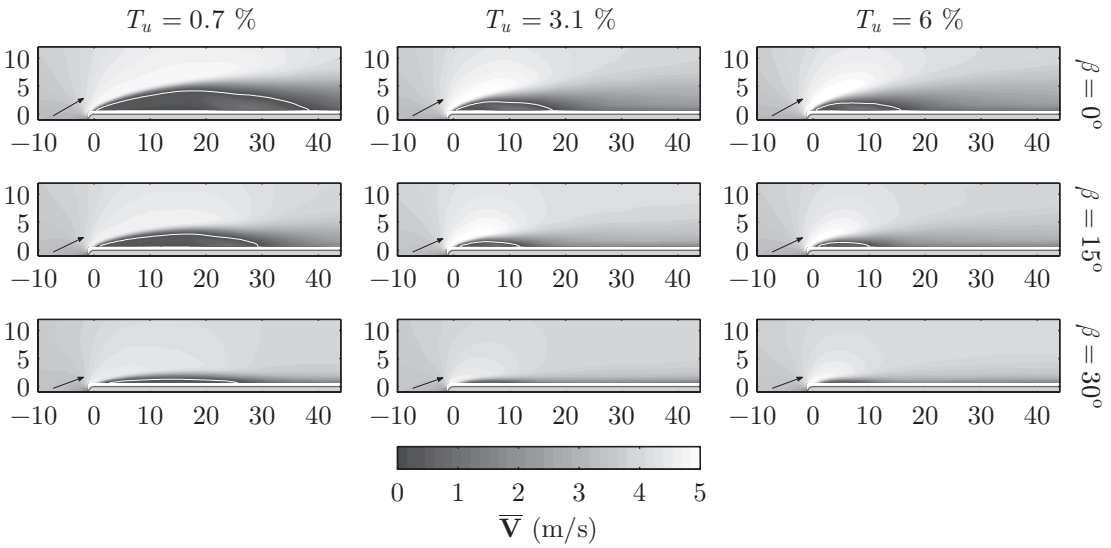

Figure 6: Time-mean absolute velocity contours of all series I bubbles (see table 1). Leading-edge flow incidence α is indicated by an arrow in each case. As per figure 5, $\overline{u}$ zero-contours are shown in white and the plate is coloured in grey. Axis units are [mm].

The bubbles for all series I cases are shown in figure 6. It is evident that increasing either the flap setting or turbulence level causes the time-mean bubble to shrink. The effect of the flap, and thus separation incidence, is an inertial one: at high flap settings, associated with shallow approach angles, 'overshoot' of the separated layer is milder and the mean reattachment length shortens. The wall also inhibits spreading of the layer [5]. Present measurements indicate that in order to remove the bubble entirely, a mildly negative approach incidence would be required—but that the bubble will, in practical terms, have diminished to immeasurably small proportions by the attached flap setting of 45°. The effect is dependent upon both leading- and trailing-edge conditions, however, and will therefore differ between facilities.

The influence of free-stream turbulence on separation bubbles has been studied by many workers (e.g. [6]) and in all cases, its presence has shortened the time-mean bubble. The operating mechanism depends on the Reynolds number, however. In the present transitional

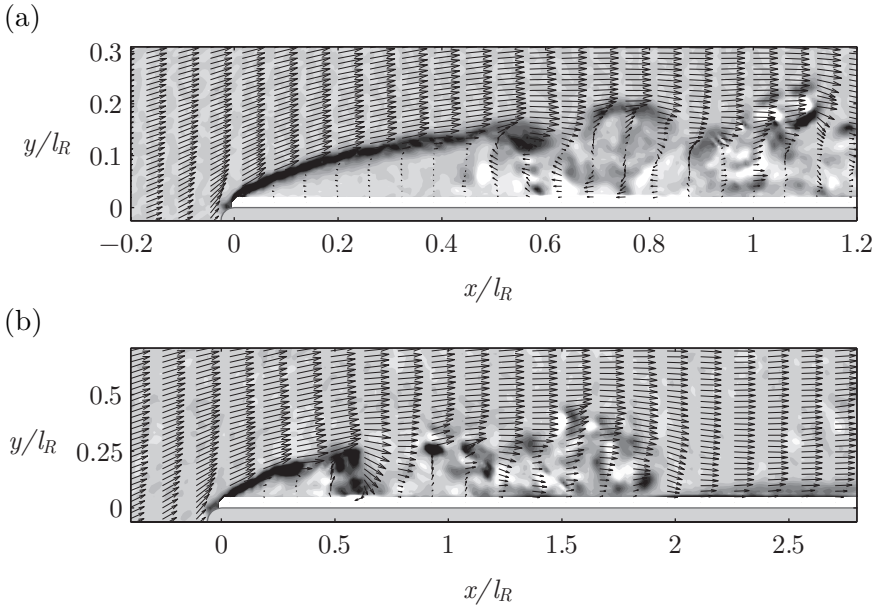

Figure 7: Snapshots of absolute velocity (vectors) and vorticity (contours) for the 0° flap bubble: (a) background and (b) high free-stream turbulence. $l_R = 39$ mm and 16.2 mm, respectively.

regime, the effect results primarily from advanced breakdown in the separated shear layer and is analogous, at least qualitatively, to the 'bypass' scenario of the attached case [7]. This is illustrated by the instantaneous flow fields of figure 7 for the 0° flap setting: under elevated free-stream turbulence, breakdown initiates at $x/l_R \approx 0.25$—as opposed to $x/l_R \approx 0.45$ in the background turbulence case—and the shear layer returns to the wall more quickly in the mean. But as shown by the contours of figure 6, the effect is one of diminishing returns and the bubble cannot be removed entirely whilst separation is forced at the leading edge.

3.2. Boundary layer development (series II)

Figure 8 shows mean boundary layer velocity profiles for all series II cases, in customary bubble-length (x/l_R) spacing. Normalised layer thickness δ_{99}/l_R (at which $\overline{u}/U_\infty = 0.99$) and Prandtl's one-seventh turbulent profile are also shown for downstream stations.

Several observations may be made on the form of the reattached layers: first, in no case do the profiles begin to settle until the initial velocity 'dip' at $y/l_R \approx 0.25$—effected by the sudden action of wall shear on the inflectional profiles at reattachment—has been smoothed out. Here, this has largely taken place by $x/l_R \approx 6$. Second, for a fixed flap setting, the addition of free-stream turbulence marginally extends the 'overshoot' of the reattachment ($x/l_R = 1$) profile. This is a result of the greater mean distortion induced by the lower aspect ratio bubble at high T_u (*cf.* figure 6). Third, by $x/l_R = 10$, both 22.5° flap layers are further from Prandtl's profile than those at the 0° flap setting. Downstream momentum thickness Reynolds numbers Re_θ ($= U_\infty\theta/\nu$, where θ is the momentum thickness) are also low—on the order of twofold lower, in fact, than those usually observed for orthodox inchoate turbulent boundary layers [8].

Figure 9 shows the shape factor H_{12} ($= \delta^*/\theta$, where δ^* is the displacement thickness and θ is as above) for each reattached wall layer. The shape factor is a measure of 'fullness' across the mean velocity profile and is well suited to the region of rapid change after reattachment (termed 'post-reattachment' herein). Under background turbulence, the 22.5° flap case is the quicker to develop initially. But as further shown by its mean velocity profiles, it is insensitive to further change after $x/l_R \approx 3$ and has settled to a high non-turbulent shape factor of 1.6 by $x/l_R = 10$.

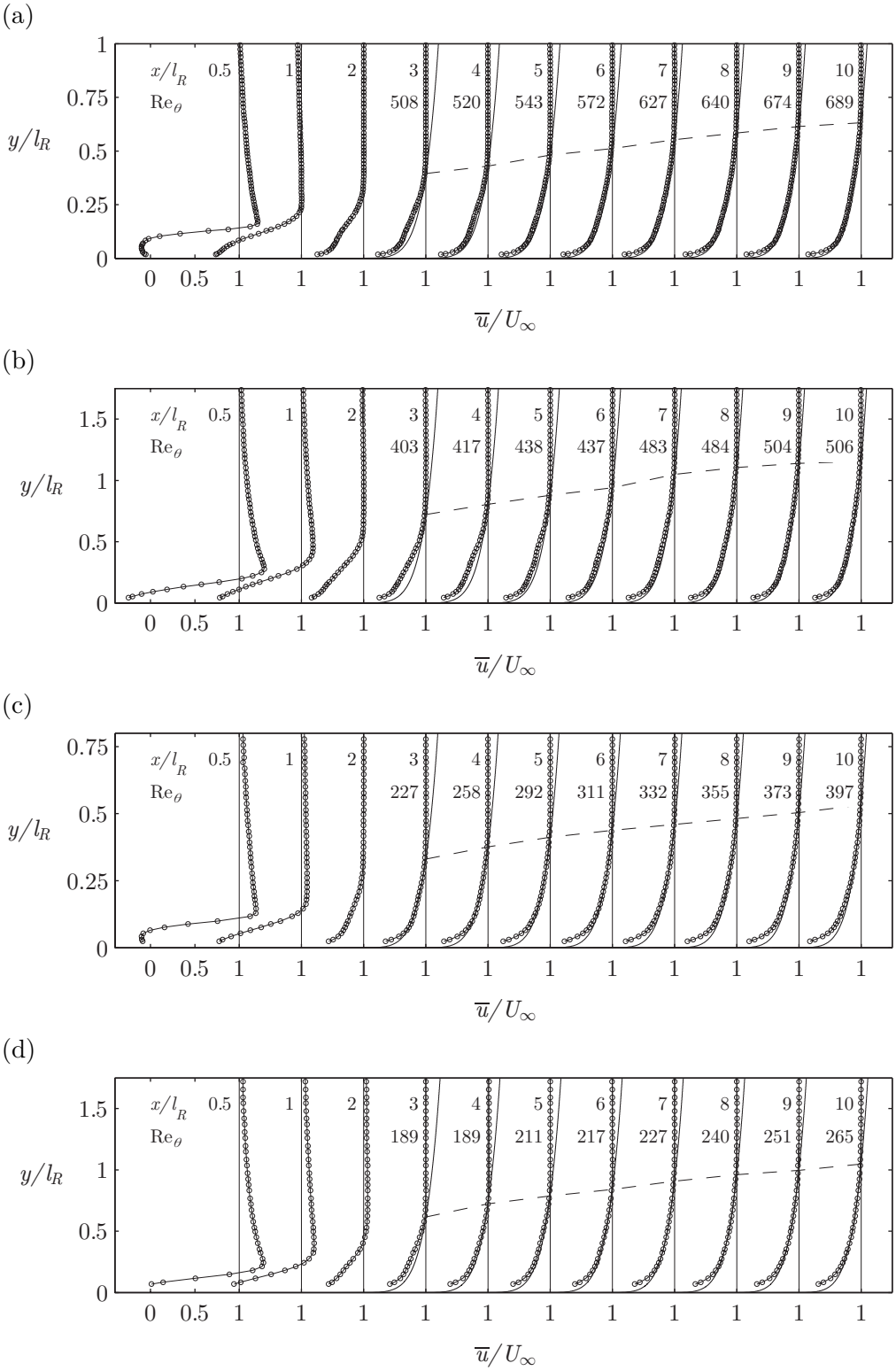

Figure 8: Normalised velocity profiles for each reattached layer. (a) $\beta = 0°$ at background T_u; (b) $\beta = 0°$ at $T_u = 5.7$ %; (c) $\beta = 22.5°$ at background T_u; (d) $\beta = 22.5°$ at $T_u = 5.7$ %. In each figure: – – – δ_{99}/l_R; —— Prandtl's turbulent profile (scaled to δ_{99}/l_R at each station). Re_θ is the boundary layer momentum thickness Reynolds number and the profile shift is $\overline{u}/U_\infty = 0.7$.

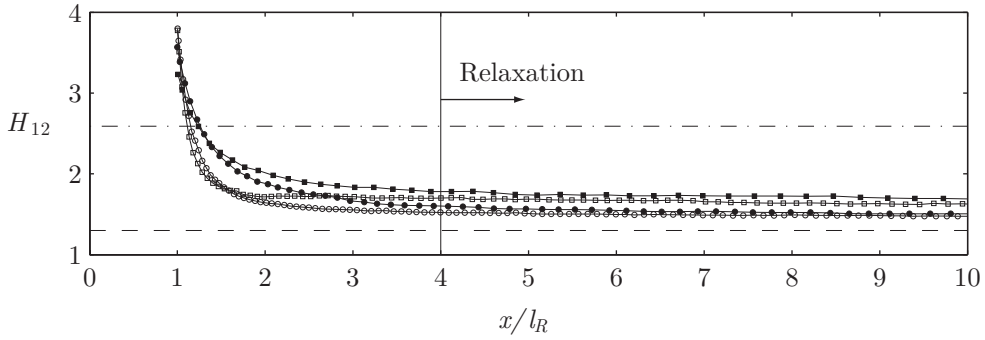

Figure 9: Decline in shape factor H_{12}. ○ $\beta = 0°$ at background T_u; ● $\beta = 0°$ at $T_u = 5.7$ %; □ $\beta = 22.5°$ at background T_u; ■ $\beta = 22.5°$ at $T_u = 5.7$ %. — · — Laminar; – – – Turbulent.

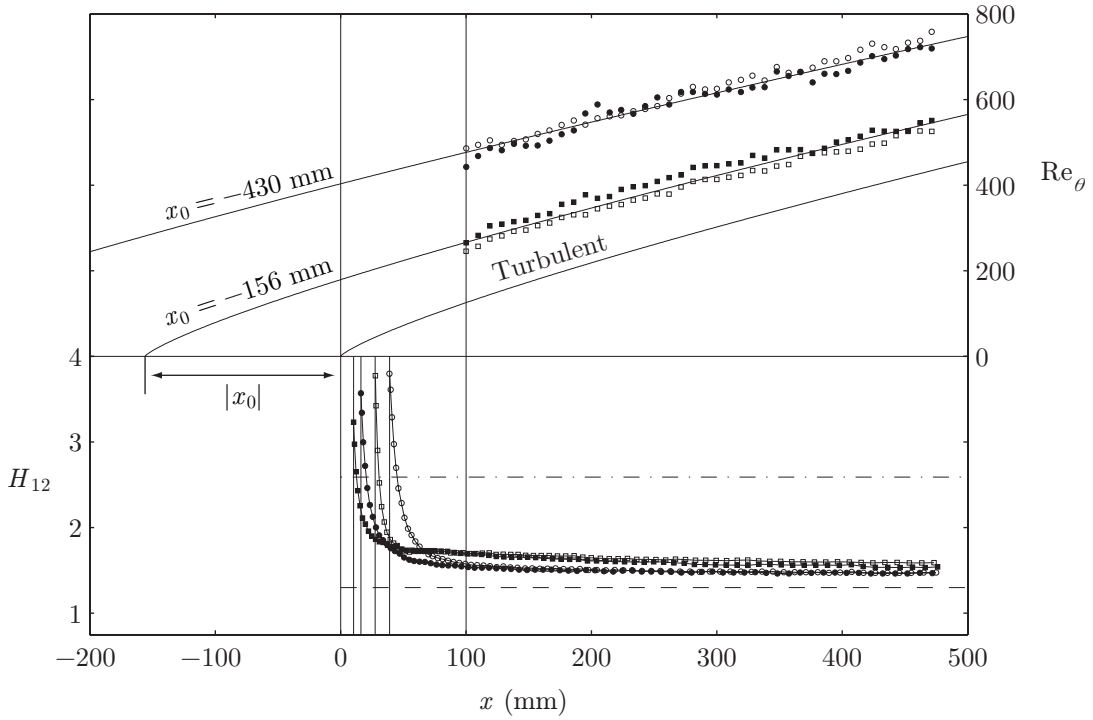

Figure 10: Evolution of momentum thickness Reynolds number Re_θ and shape factor H_{12} with physical streamwise distance x. Upper plot: —— Equation 1 (for various virtual origins x_0). In the lower plot, vertical lines across $0 < x < 50$ mm signify reattachment for each case. See figure 9 for marker symbols.

Under free-stream turbulence, both cases develop similarly at first but (a) level out more slowly and (b) eventually plateau to higher shape factors than the background turbulence cases. This result—that free-stream turbulence should mildly *delay* mean development in bubble-length terms—is somewhat counter-intuitive, but has also been observed over blunt-nosed flat plates e.g. Castro & Epik [2] found that the aforementioned velocity dip, which corresponds to a higher shape factor, was more pronounced under turbulence (*cf.* figure 8).

Downstream of post-reattachment, further change is practically undetectable in all cases and as shown in figure 10, none has reached a turbulent value ($H_{12} \approx 1.3$ for Prandtl's profile, although often nearer 1.4 in practice) by the last station.

Although bubble-length scaling (i.e. x/l_R) is frequently used in separation-reattachment flows, here it masks the fact that downstream of post-reattachment each flap setting behaves similarly in dimensional terms. This is illustrated in figure 10 with a stacked plot of momentum thickness Reynolds number Re_θ and shape factor H_{12}. The data are plotted against streamwise coordinate x from the leading edge. Also shown for each Re_θ set is the standard formula for an attached turbulent boundary layer [9] but with the inclusion of a virtual origin x_0:

$$\mathrm{Re}_\theta = 0.036\left(\frac{U_\infty}{\nu}\right)^{\frac{4}{5}}(x - x_0)^{\frac{4}{5}}. \tag{1}$$

U_∞ is the nominal free-stream velocity *above* the plate (which differs slightly from U_I due to the acceleration around the leading edge and bubble) and is approximately constant at 4 m/s for $x > 100$ mm. Three origins are shown: (i) $x_0 = 0$ mm (a regular turbulent boundary layer growing from the leading edge); (ii) $x_0 = -156$ mm; and (iii) $x_0 = -430$ mm.

At both flap angles, Re_θ develops almost independently of the turbulence level and although none of the constituent cases—especially those at the 22.5° setting—is canonically turbulent in the mean, streamwise growth can be correlated by shifted turbulent curves with origins (ii) and (iii). In combination with corresponding shape factors from the lower part of the figure, it follows that neither an accelerated transition (*cf.* figure 7) nor additional downstream forcing significantly affect growth of the layer beyond post-reattachment. The area-averaged drag coefficient C_f for $100 < x < x_{max}$ (mm) is therefore almost identical in both cases.

To a first order, it is also possible to estimate the heat transfer characteristics of the reattached layer by the *Reynolds-Colburn* analogy. Local skin-friction coefficient C_{fx} can be related to the Stanton number St_x by [10]:

$$\mathrm{St}_x\mathrm{Pr}^{\frac{2}{3}} = \frac{C_{fx}}{2}. \tag{2}$$

Pr is the Prandtl number. Local skin-friction coefficients were thus derived by the Clauser chart method [11] and a Coles-type fitting procedure [12]. This was possible only for the 0° flap cases for $x > 100$ mm, however, since the standard inner log law ($u^+ = 2.44 \ln y^+ + 5.0$; [9]) did not exist for most of both 22.5° flap cases—despite apparent similarities in outer growth to a shifted turbulent boundary layer.

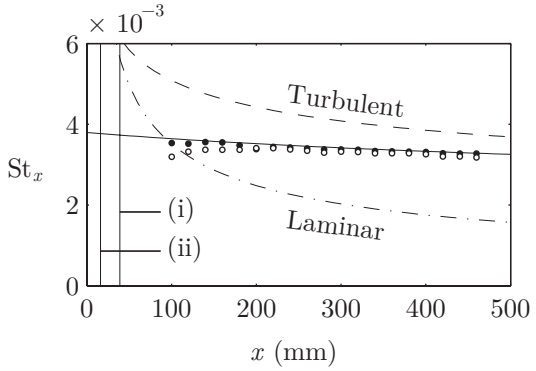

Figure 11: Development of local Stanton number St_x with distance x for both 0° flap cases. — · — Equation 3; – – – Equation 4; —— Equation 5. See figure 9 for marker symbols. Note (i) and (ii) are the bubble lengths for background and elevated turbulence cases, respectively.

Figure 11 shows the corresponding Stanton number distributions for $x > 100$ mm alongside the iso-flux laminar (L):

$$\left(\mathrm{St}_x\right)_L = 0.453\mathrm{Pr}^{-\frac{2}{3}}\left(\frac{U_\infty}{\nu}\right)^{-\frac{1}{2}}x^{-\frac{1}{2}} \tag{3}$$

and turbulent (T) relations:

$$\left(\mathrm{St}_x\right)_T = 0.0308\mathrm{Pr}^{-\frac{2}{3}}\left(\frac{U_\infty}{\nu}\right)^{-\frac{1}{5}} x^{-\frac{1}{5}} \tag{4}$$

for attached flat-plate boundary layers growing from the leading edge [10]. Also plotted for comparison is the shifted turbulent (TS) curve:

$$\left(\mathrm{St}_x\right)_{TS} = 0.0308\mathrm{Pr}^{-\frac{2}{3}}\left(\frac{U_\infty}{\nu}\right)^{-\frac{1}{5}} (x - x_0)^{-\frac{1}{5}} \tag{5}$$

where $x_0 = -430$ mm, as per figure 10.

The results for both reattached layers lie above the laminar line. From a heat transfer perspective, the question therefore arises as to whether it might be beneficial, for those flows at sufficiently high Reynolds numbers that would otherwise be attached and laminar, to *force* separation (e.g. with a flap or actuated surface) and trip the boundary layer into a 'quasi-turbulent' state. This would effect a faster transition than that induced by free-stream turbulence alone (indeed the turbulent correlation, although shown here for comparison, would not usually apply until further downstream). The corollaries, though, are: (a) a probable rise in system pressure drop, and (b) a reduction in heat transfer around the bubble and post-reattachment zones due to circulation and low mean wall gradients. And although, as shown in section 3.1, free-stream turbulence serves to shrink these bubble regions, it has minimal impact beyond post-reattachment (figures 10 and 11) and should probably be avoided if an additional energy penalty must be incurred.

4. Summary & Conclusions

High-resolution Particle Image Velocimetry (PIV) data have been presented for the separation-reattachment flow over a round-nosed flat plate. Focus is given to the effects of flow approach angle (manipulated via a trailing edge flap) and free-stream turbulence (generated by grids) on both mean aerodynamic and heat transfer characteristics. Salient conclusions are as follows:

(i) In the first series of measurements (I) it was found that an increase in either flap setting (corresponding to a decrease in the approach angle) or free-stream turbulence level caused the time-mean separation bubble to shrink. The effect was monotonic in both variables and one of diminishing returns.

(ii) Under free-stream turbulence, instantaneous PIV snapshots revealed that an *accelerated* transition mechanism was responsible for shortening the bubble.

(iii) In the second series of measurements (II) it was found that in all test cases, relaxation of the reattached boundary layer unfolded rapidly at first but reached a plateau approximately three bubble-lengths downstream of reattachment.

(iv) Local momentum thickness Reynolds and Stanton numbers for each flap setting were found to develop independently of the free-stream turbulence level for $x > 100$ mm and could be described by shifted turbulent correlations. In this region, heat transfer performance is expected to be superior to regular laminar flow.

A detailed perspective on the underlying mechanics of this separated flow will be presented in a future paper.

Acknowledgments

Funding support from the Irish Research Council (IRC) is gratefully acknowledged. Bell Labs Ireland would also like to thank the Industrial Development Agency (IDA) Ireland for their continued support.

References

[1] Ota T, Asano Y and Okawa J 1981 *B. JSME* **24** p 944
[2] Castro I P and Epik E 1998 *J. Fluid Mech.* **374** 91–116
[3] Ruderich R and Fernholz H H 1986 *J. Fluid Mech.* **163** 283–322
[4] Roach P E 1987 *Int. J. Heat Fluid Fl.* **8** 82–92
[5] Bearman P W and Morel T 1983 *Prog. Aerospace Sci.* **20** 97–123
[6] Kalter M and Fernholz H H 2001 *J. Fluid Mech.* **446** 271–308
[7] Langari M and Yang Z 2013 *Phys. Fluids* **25**
[8] Castro I P 1984 *J. Fuid Eng.—T. ASME* **106**
[9] Schlichting H 1979 *Boundary Layer Theory* (New York: McGraw-Hill)
[10] Holman J P 2010 *Heat Transfer* (New York: McGraw-Hill)
[11] Clauser F H 1954 *J. Aeronaut. Sci.* 91–108
[12] Coles D E 1962 *The Turbulent Boundary Layer in a Compressible Fluid* R–403–PR (RAND: California)
[13] Mayle R E and Bellows W J 1986 *J. Turbomach.* **108** 131–136